Journal of Magnetic Resonance **144,** 142–149 (2000)
doi:10.1006/jmre.2000.2027, available online at http://www.idealibrary.com on IDEAL®

# Combining PGSE NMR with Homonuclear Dipolar Decoupling

S. V. Dvinskikh[1] and I. Furó[2]

*Division of Physical Chemistry, Department of Chemistry, Royal Institute of Technology, SE-10044 Stockholm, Sweden*

Received November 12, 1999; revised January 18, 2000

**A new robust approach for combining multiple-pulse homonuclear decoupling and PGSE NMR is introduced for accurately measuring molecular diffusion coefficients in systems with nonvanishing static homonuclear dipolar couplings. Homonuclear decoupling suppresses dipolar dephasing during the gradient pulses but its efficiency and scaling factor for the effective gradient vary across the sample because of the large variation of the frequency offset caused by the gradient. The resulting artifacts are reduced by introducing a slice selection scheme. The method is demonstrated by $^{19}$F PGSE NMR experiments in a lyotropic liquid crystal.** © 2000 Academic Press

*Key Words:* **PGSE NMR; homonuclear dipolar decoupling; slice selection; molecular diffusion; liquid crystal.**

## INTRODUCTION

Nowadays PGSE-type NMR experiments (for simplicity, hereafter referred to as PGSE) (*1–6*) are used routinely for studying molecular self diffusion in isotropic liquids. The same method is far less suitable in liquid crystals or in solids. In those materials, nonvanishing static dipolar coupling causes fast dephasing of the transverse magnetization and any extra dephasing induced by diffusion in the applied field gradient is negligible. It is a straightforward idea to use dipolar decoupling to lengthen the decay of transverse magnetization (*7–9*). In contrast to other methods, such as using ultra-high-static magnetic field gradients (*10*) or samples macroscopically oriented at the magic angle to the static field (*11–14*), combining decoupling with PGSE preserves the flexibility of the latter technique and demands no cumbersome sample preparation.

In early approaches to diffusion measurements with homonuclear decoupling (*7, 8*), field gradient pulses were applied in the time windows between the radiofrequency (RF) pulses of the decoupling sequence. Since those windows were typically 10 $\mu$s long, the gradient strength and, consequently, the available diffusion coefficient were very limited. Later, this approach has been extended to measure spin diffusion via static dipole couplings (*15*). It has only been recently that multiple-pulse homonuclear decoupling was applied *simultaneously* with a large, although static, magnetic field gradient to measure slow diffusion in plastic crystals (*9*). Combinations of heteronuclear dipolar decoupling with PGSE have been also presented (*16, 17*).

While PGSE with heteronuclear decoupling might be easier to implement (*17*), that method has the disadvantage of detecting the NMR signal from a usually low-abundance, low-$\gamma$ nucleus. In contrast, PGSE with homonuclear decoupling is attractive because it can detect abundant nuclei with high gyromagnetic ratio. Hence, measuring the molecular diffusion in systems with small signal-to-noise ratio (e.g., in less concentrated systems) may demand this latter experiment. There is a multitude of well-developed techniques for multiple-pulse homonuclear dipolar decoupling in solids (*18–25*), and in solid state magnetic resonance imaging (*26–28*) they have been applied in combination with static or pulsed magnetic field gradients (although at gradient values insufficiently small for measuring diffusion). In the article (*9*) that initiated the present work, the well-known MREV-8 decoupling sequence has been combined with a strong static gradient and was shown that the technique is indeed viable. As a particularly important point, the reduction of the signal-to-noise ratio by the large gradient was tolerable in that work because the (effective) transverse relaxation time $T_2^*$ has been prolonged in a number of slices of the excited sample volume by the far-off-resonance averaging effect (*29*).

In this paper, homonuclear dipolar decoupling is applied *during* pulses of magnetic field gradient. Our aim is to extend the range of anisotropic systems, particularly lyotropic liquid crystals, in which molecular diffusion coefficients can be measured. The design should operate at relatively fast ($10^{-12}$–$10^{-10}$ m$^2$/s) diffusion coefficients available at the gradient strength of commercial gradient probes with encoding times (conventionally denoted as $\delta$) in the order of milliseconds and diffusion times ($\Delta$) in the order of 100 ms–1 s (see Fig. 1). There are two particularly important design criteria. First, lyotropic liquid crystals are usually highly conductive and therefore very susceptible to RF-induced heating. To avoid significant changes in the state of the sample, the temperature shift and temperature

[1] On leave from the Institute of Physics, St. Petersburg State University, 198904 St. Petersburg, Russia.

[2] To whom correspondence should be addressed. Fax: +46 8 7908207. E-mail: ifuro@physchem.kth.se.



1090-7807/00 $35.00

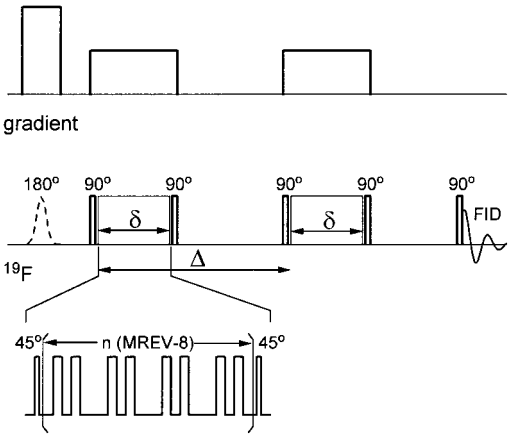


**FIG. 1.** $^{19}$F PGSE NMR with a stimulated echo–LED pulse sequence combined with MREV-8 homonuclear dipolar decoupling and slice selection. The slice selection is performed before the stimulated echo sequence with a selective inversion pulse during an additional gradient pulse. The inversion pulse is absent in every second scan and two subsequent FIDs are subtracted so that the signal from $z$-magnetization in the selected slice is summed, while it is canceled outside this region. The width of the excited slice is adjusted to include the region within which the scaling factor $s$ is constant to a desired accuracy.

distribution within the sample must be typically kept below 1 K during the experiment. This factor limits the applicable RF decoupling power. Second, to answer questions about the structure of the investigated material, the diffusion coefficient must be measured with an accuracy of a few percent. This presumably requires that the effective field gradient (which is scaled down by homonuclear decoupling) is homogeneous over the part of the sample volume that contributes to the collected signal. These aspects have not yet been investigated thoroughly enough. In the present contribution we report such an investigation that results in a new design for PGSE experiments with homonuclear decoupling. The basic principle, slice selection, is the same as in our implementation (*17*) of PGSE (in particular, a stimulated-echo-type experiment) with heteronuclear decoupling. The method is demonstrated on the same (*17*) sample, the lyotropic mixture of cesium perfluorooctanoate (CsPFO)–water (*30*).

## METHOD

One faces a particular problem when implementing homonuclear decoupling in a diffusion experiment. In the presence of a field gradient $g$, different parts of the sample experience different magnetic field strengths, which leads to a position-dependent resonance frequency offset across the sample volume. First, this causes a corresponding variation of the decoupling efficiency. Second, the applied field gradient is scaled by the so-called scaling factor $s$ of a decoupling sequence that reduces linear spin operator terms such as chemical shift. Since $s$ varies with the frequency offset, the effective field gradient, experienced by spins, becomes inhomogeneous across the sample.

The first effect leads to a loss of NMR signal since transverse magnetization from imperfectly decoupled sample regions decays completely during $\delta$ and, therefore, does not contribute to the collected signal. The second effect is an inhomogeneous attenuation of the signal by diffusion. It was shown (*29*) that far-off-resonance averaging partially compensates for the signal loss. It was also suggested (*29*) that the contribution from regions with scaling factors $s$ different from the on-resonance value $s_0$ is insignificant in a diffusion experiment. The argument is that regions with $s \neq s_0$ are, at the same time, regions with ineffective decoupling. Hence, one could approximate the effective field gradient in a diffusion experiment as $g_{\text{eff}} = s_0 \cdot g$. However, as shown below, this procedure may introduce large errors. Indeed, both the scaling factor and the decoupling efficiency change smoothly with the frequency offset and not on a stepwise manner as the previous argument would suggest. Therefore, we observe a reduction of the apparent diffusion coefficient with increasing gradient strength (since $s$ decreases with resonance offset). This behavior is a clear signature that regions with scaling factor lower than the on-resonance value and with lower-than-optimal decoupling efficiency contribute significantly to the detected signal. If accuracy is an issue, this variation of the scaling factor cannot be neglected. One could, in principle, correct for this effect, but in practice that would be difficult since it requires measuring the detailed offset dependence of the scaling factor and the effective transverse relaxation time $T_2^*$. Thus, the straightforward combination of PGSE with homonuclear decoupling as implied by (*9*) is not suitable in this case.

A simple way to reduce the influence of the variation of the decoupling effect is to involve slice selection, well known from magnetic resonance imaging (*4*). The approach is similar to that one used in (*17*) for the PGSE experiment with heteronuclear decoupling. Slice selection cancels the signal from regions with large resonance offset so that the measurement is representative to that part of the sample where the scaling factor $s$ is well defined (close to $s_0$). In the most straightforward modification of PGSE, at least two of the hard 90° pulses of the pulse sequence are replaced by soft 90° pulses and the gradient pulses are extended so that soft pulses during them perform the slice selection. However, we found it more practical to perform the slice selection before the PGSE sequence by applying a soft inversion pulse as depicted in Fig. 1.

The actual pulse sequence is derived from the standard stimulated echo experiment (*2*), supplemented by "longitudinal eddy delay" (LED) (*31*). The dipolar dephasing during the gradient pulses is suppressed by multiple-pulse homonuclear decoupling, as suggested in Ref. (*9*). The selective inversion pulse, applied during an additional gradient pulse, is absent in every second scan and the subsequent FIDs are subtracted so

that the signal arising from the $z$ magnetization within the selected bandwidth is summed, while that is canceled outside this region. The bandwidth of the selective pulses is adjusted to excite only that central region of the sample where the scaling factor is close to its on-resonance value. The narrower the selected bandwidth is the higher the homogeneity of the scaling factor achieved. A practical lower limit for the bandwidth is the width of the undecoupled spectrum. (Exciting a narrow band with a long soft pulse may create multiple quantum coherences and multispin polarizations whose effect, if necessary, can be filtered out but by longer phase cycles (*32, 33*).)

This slice selection scheme is better than the direct incorporation of soft 90° pulses in the stimulated echo experiment; in particular, the signal-to-noise ratio is higher because the effect of transverse relaxation is reduced. The advantages come because (i) only one selective pulse is required, while the direct incorporation of slice selection requires at least two selective 90° pulses to get equivalent encoding and decoding periods ($\delta$ in Fig. 1); (ii) a selective inversion pulse is typically shorter than a selective excitation pulse of the same bandwidth (*34*); (iii) transverse relaxation is less effective during an inversion pulse; (iv) since the strength of the first gradient pulse can be set independently from the gradient applied during the encoding/decoding periods, the selected bandwidth can be flexibly adjusted and/or the soft 180° pulse can be kept short; and (v) there is no need to correct the value of $\delta$ for partial encoding/decoding during selective pulses.

Diffusion experiments with homonuclear decoupling cannot proceed by recording the variation of the signal intensity on increasing gradient strength, because the variation of the gradient would correspondingly modify the decoupled sample volume and, hence, the signal intensity. Varying the length of delay $\delta$ is also impractical as it would vary the heating effect from the decoupling. Thus, the only remaining option is to record the decay of the signal with increasing $\Delta$ just as in the PGSE experiment with heteronuclear decoupling (*17*). The result is (*2*)

$$S(\Delta) \sim \exp(-R \cdot \Delta) \qquad [1a]$$

with

$$R = (\gamma s g \delta)^2 D + 1/T_1. \qquad [1b]$$

The difference between the decay constants recorded with different gradients $g$ provides one with the diffusion coefficient $D$.

One disadvantage of the method is the loss of signal intensity due to detection of signal from only one slice of the sample. In (*17*) a sequential slice selection scheme was used to recover that loss; the frequencies of the soft excitation pulses ($^{13}$C) and *heteronuclear* decoupling ($^{19}$F) were stepped synchronously to collect $^{13}$C signal from the adjacent regions of the sample. This scheme cannot be applied here because the fluorine spins of the whole sample are disturbed during *homonuclear* decoupling. Nevertheless, the overall sensitivity of the method is still high due to 100% natural abundance and high gyromagnetic ratio of the selected nuclei that can be $^{19}$F for $^{1}$H.

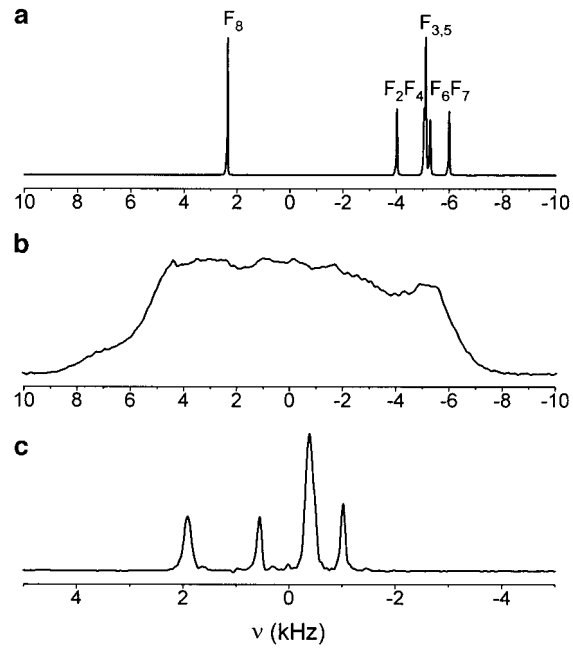


**FIG. 2.** $^{19}$F NMR spectra of CsPFO/$D_2O$ (at 50 wt%) in the isotropic phase at 325 K (a) and in the nematic phase at 315 K (b, c), recorded at 188 MHz. The nematic sample is uniformly oriented by the magnetic field with its director parallel to the field direction. Spectrum (c) is recorded in the presence of MREV-8 homonuclear decoupling with 2.6 $\mu$s 90° pulse length and 84 $\mu$s cycle time. Note that the frequency scale for spectrum (c) is not corrected by the scaling factor $s$ ($\approx$0.5). The spectra were recorded with the same RF offsets.

## RESULTS AND DISCUSSION

### *$^{19}$F Spectra of the Test Sample*

The $^{19}$F NMR spectra of CsPFO in $D_2O$, recorded at 188 MHz, are shown in Fig. 2. The isotropic liquid spectrum, recorded at 325 K and shown in Fig. 2a, is assigned as previously communicated (*35*). The spectra of the nematic phase at 315 K, recorded without and with homonuclear decoupling, are shown in Figs. 2b and 2c, respectively. The oblate-shape micelles in the nematic phase are oriented with their short axes parallel to the magnetic field. The relative chemical shifts of the fluorine lines are clearly different in the two spectra of Figs. 2a and 2c. As explained in detail in (*17*), the line positions in the isotropic micellar phase reflect the isotropic averages of the respective molecular chemical shift anisotropy (CSA) tensor. In the nematic phase, they instead depend on the principal values ($\sigma_{zz}$) of those CSA tensors

**TABLE 1**
**Scaling Factors and Frequency Offset Ranges for MREV-8**

| Cycle time[a] ($\mu$s) | $s_0$ Calculated[b] | $s_0$ Measured (see Fig. 3) | Offset range[c] (kHz) |
|---|---|---|---|
| 60 | 0.505 | 0.507 ± 0.005 | ±16 |
| 84 | 0.495 | 0.502 ± 0.006 | ±11 |
| 120 | 0.488 | 0.496 ± 0.006 | ±7 |
| 480 | 0.476 | 0.489 ± 0.010 | ±2 |

[a] 90° pulse length 2.6 $\mu$s.
[b] From Ref. (*19*).
[c] For $s$ within ±5% of $s_0$.

reduced both by molecular motions and by the homonuclear decoupling.

*Calibration of the Scaling Factor*

In the pulse sequence in Fig. 1, the applied field gradient $g$ is reduced to the effective gradient $s \cdot g$ by homonuclear decoupling (see Eq. [1]). The theoretical on-resonance values of the scaling factor $s$ (*19*) at different lengths of 90° pulses and with different decoupling cycle times for MREV-8 (*18, 19*) are shown in Table 1. The offset-dependence of $s$ was measured with the $^{19}$F RF power set relatively low ($\gamma B_1/2\pi \approx 96$ kHz, 2.6-$\mu$s length of the 90° pulse) to avoid excessive sample heating. The experimental scaling factors were first determined in the isotropic micellar phase by observing the frequency shift $\nu'$ of the $^{19}$F lines under decoupling upon shifting the RF offset by $\nu$. The $s = \nu'/\nu$ data are displayed in Fig. 3. The extrapolated on-resonance values, given in Table 1, are close to the theoretical figures. Clearly, the shorter the cycle length is, the less offset-dependent is the scaling factor. At longer cycle times, we observe an oscillatory behavior that agrees qualitatively with the theoretical results of (*29*) while there is some quantitative deviation caused by the nonideality and finite length of the RF pulses. The offset dependence of the scaling factor $s$ has also been measured in the nematic and lamellar phase of CsPFO/$D_2O$; no significant differences to the isotropic case were found as demonstrated in Fig. 3b. Scaling factors measured for different fluorine positions in the surfactant molecule coincide within experimental error.

Using Fig. 3, one can choose the frequency offset range within which the scaling factor is constant by the desirable accuracy and the width of the selected slice can be adjusted to this range. The offset range within which the scaling factor varies less than 10% is indeed given in Table 1. In principle, the $s(\nu)$ profile could also be used to obtain an effective gradient value even if a wide frequency range is excited with substantially varying $s$. However, $T_2^*$ also strongly varies with the decoupling offset and therefore the $s(\nu)$ profile should be weighted by the exponential factor $\exp(-\delta/T_2^*(\nu))$. The $T_2^*(\nu)$ profiles are different for different fluorines and vary with temperature so that such a correction is impractical.

*Results of the Diffusion Experiments*

The influence of slice selection on the diffusion decay is demonstrated in Fig. 4, where the experimental results in the isotropic and nematic phases of CsPFO/$D_2O$ are shown. The experiments were performed with field gradients perpendicular to the $B_0$ field and $\delta = 1.8$ ms (set shorter than the average $T_2^* \approx 3$ ms in nematic phase under decoupling). In the isotropic phase (Fig. 4a, with $g = 76$ G/cm that corresponds to ±61 kHz offset distribution in our ≈4-mm-id sample) a fast decay is observed in the absence of decoupling; the line is a single exponential fit. The experiment with MREV-8 decoupling and without slice selection produces a slow decay, while introducing the slice selection results in a faster decay (see Fig. 4a). This is a clear fingerprint of the variation of the scaling factor $s$ with the frequency offset. In the experiment without slice selection the signal is contributed by all parts of the sample, even by ones with smaller scaling factors. In the slice-selected

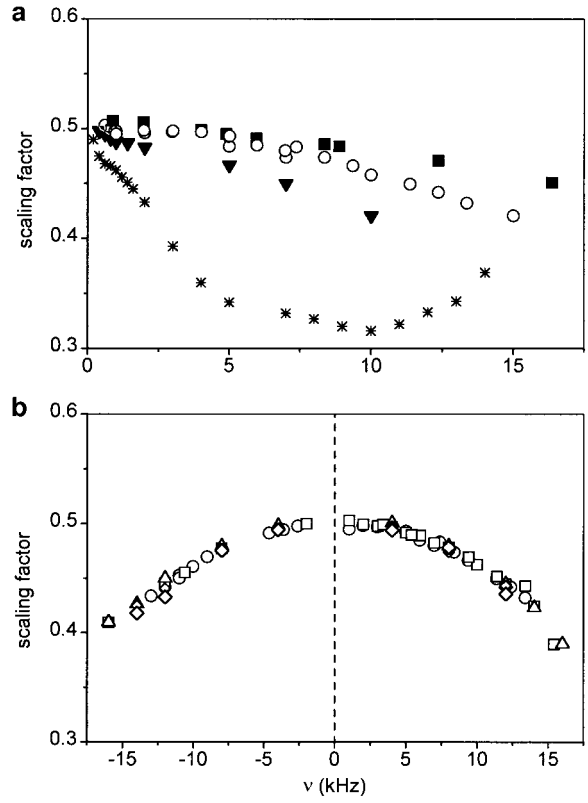


**FIG. 3.** Offset dependence of the experimental scaling factor $s$ for MREV-8 in CsPFO/$D_2O$. (a) Isotropic phase at 325 K. Cycle times are 60 $\mu$s (■), 84 $\mu$s (○), 120 $\mu$s (▼), and 480 $\mu$s (∗) and the length of the 90° pulse is 2.6 $\mu$s. (b) Comparison of the scaling factor $s$ in different phases of CsPFO/$D_2O$ at 84 $\mu$s cycle time: isotropic at 325 K (○), nematic at 318 K (□), nematic at 315 K (△), lamellar at 309 K (◇).

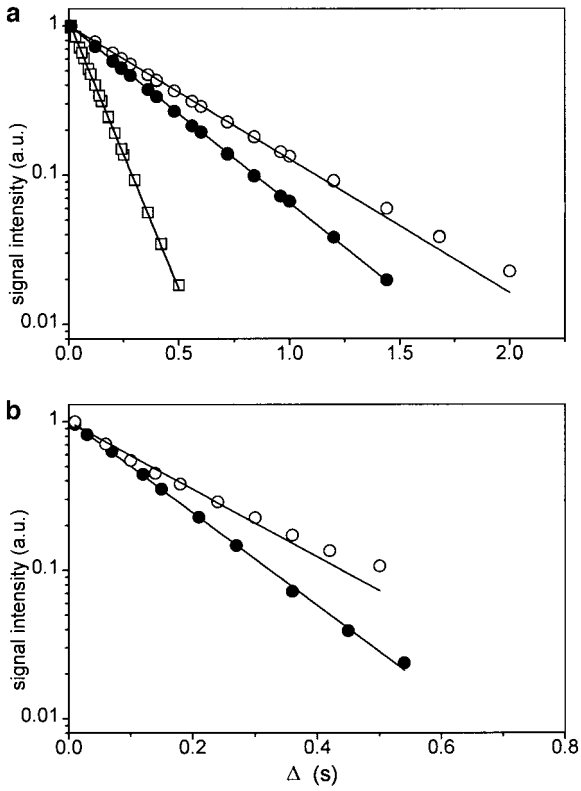


**FIG. 4.** Variation of the $^{19}F$ signal intensity in CsPFO/$D_2O$ (50 wt%) with increasing delay time $\Delta$ in the PGSE experiment depicted in Fig. 1. The MREV-8 decoupling was performed with 2.6-$\mu$s-long 90° pulses and 60-$\mu$s-long cycles; 30 cycles were applied during the $\delta = 1.8$ ms gradient pulses. The solid symbols represent data recorded with slice selection by a soft Gaussian pulse; open symbols are data points with no slice selection (the selective pulse in Fig. 1 is replaced by a hard 180° pulse). The lines are single-exponential fits to Eq. [1]. (a) Isotropic phase at 325 K, $g = 76$ G/cm, without (□) and with (○, ●) decoupling. (b) Nematic phase at 315 K, $g = 114$ G/cm.

experiment, only the central slice of the sample with small frequency offset contributes, and here the average scaling factor and the corresponding effective gradient are close to their maximum on-resonance value. This difference should be less pronounced in the anisotropic phases with nonvanishing dipolar coupling where a less effective dipolar decoupling under off-resonance condition results in shorter $T_2^*$ times, making the regions with small scaling factor contribute less to the signal. Nevertheless, we find a significant difference between the diffusion decays with and without slice selection (Fig. 4b). Note that the decay in the experiment without slice selection is also clearly nonexponential.

In Fig. 5 the experimental decay constants in nematic phase (at 315 K) are plotted as function of $(g\delta)^2$. In Fig. 5a results from experiments with and without slice selection are compared. The expected linear dependence is not observed in the experiment without slice selection (Fig. 5a, open symbols) because the average scaling factor decreases with increasing gradient strength. Limiting the excitation bandwidth to 20 kHz results in a linear behavior (solid symbols), as predicted by Eq. [1]. This point is further supported by Fig. 5b where the decay constants obtained at different $\delta$ times and different field gradient values fall on the same slope. The maximum systematic error in the slice selection approach is estimated to be $\pm 6\%$ (see profile in Fig. 3a at 60-$\mu$s cycle time), since $s$ is constant to $\pm 3\%$ within the excitation bandwidth. The effect of decreasing $T_2^*$ with the resonance offset makes the actual error even smaller.

The explicit value of the diffusion coefficient $D_\perp$ is obtained, as shown by Eq. [1], from the difference of the rate constants in measurements with different applied gradients (or, equivalently, from the slopes in Fig. 5). In the nematic phase at 315 K we thus get $D_\perp = (0.88 \pm 0.02) \times 10^{-10}$ m$^2$/s by taking the scaling factor to $s = 0.495$ (average in the range from 0 to 10 kHz). All of the measured $D_\perp$ values are shown in Fig. 6. The data agree well with the ones obtained in the same system by $^{13}C$ PGSE diffusion measurements with heteronuclear decoupling (*17*). Note that the precision is comparable in those two different experiments but the $^{19}F$ PGSE

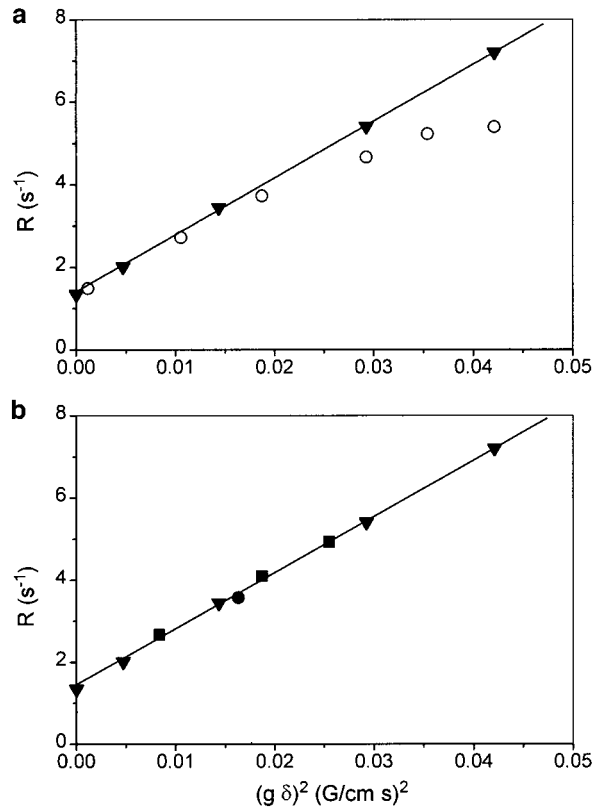


**FIG. 5.** Decay rates $R$ versus $(g\delta)^2$ in the nematic phase at 315 K as obtained from the diffusion experiment in Fig. 1. The symbols represent experimental data recorded at different experimental conditions with gradient strength $g$ up to 114 G/cm and the lines are linear fits. Parameters of MREV-8 decoupling and selective pulse are given in Fig. 4. (a) Results obtained with (▼) and without (○) slice selection and $\delta = 1.8$ ms. (b) Results obtained with slice selection at different $\delta$ values 1.8 ms (▼), 1.2 ms (■), and 0.96 ms (●).

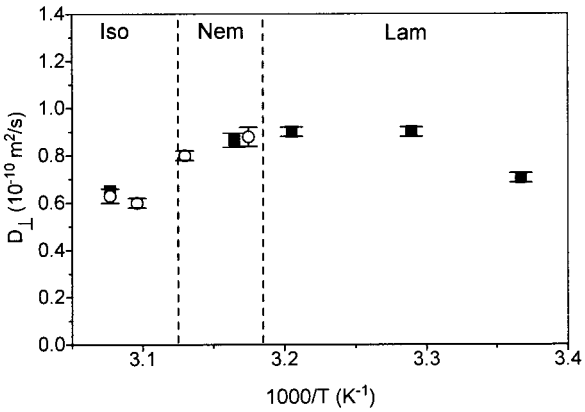


**FIG. 6.** Temperature dependence of the diffusion coefficient $D_\perp$ across the isotropic, nematic, and lamellar phases of CsPFO/$D_2O$ as measured by $^{19}F$ PGSE NMR with homonuclear decoupling in the present work (○) or by $^{13}C$ PGSE NMR with heteronuclear decoupling in Ref. (*17*) (■).

experiment with homonuclear decoupling experiment took one order of magnitude less time (that is still about 1–2 h, though).

## CONCLUSION

In this paper, we propose and demonstrate a method for accurately measuring the molecular self diffusion coefficients in systems with strong static dipolar interactions. The method is a PGSE-type experiment with homonuclear decoupling. While it is straightforward to apply homonuclear decoupling to prolong the dephasing of the transverse magnetization, the inherent offset dependence of the scaling factor and of the decoupling efficiency presents a problem. We suggest slice selection as a remedy.

The implementation of the method is not difficult on modern commercial spectrometers and there is, in principle, no need for any additional nonstandard equipment. Clearly, the accuracy achieved by slice selection is at the expense of decreasing signal-to-noise ratio. The smaller the diffusion coefficient to be measured is, the higher the signal loss; the reason is the requirement of the larger applied gradient strength which gives the excited band a smaller volume. This puts a limit on the diffusion coefficient available by this method. With our present experimental setup and in a conductive sample, diffusion coefficients in the range of $10^{-11}$–$10^{-10}$ $m^2/s$ can be measured with the accuracy of a few percent in less than 2 h of experimental time. This is much faster than that by $^{13}C$ PGSE NMR with heteronuclear dipolar decoupling (*17*).

Lower diffusion coefficients and/or shorter experimental times can be achieved in several ways. First, shortening the cycle time in the decoupling sequence (at higher average decoupling power) allows a flatter scaling factor profile and, correspondingly, broader excitation width. Second, other well-known sequences such as BR-24 and BLEW-48 could be used instead of MREV-8 to provide, although with a smaller scaling factor, a flatter scaling factor profile than that in Fig. 3 and a better decoupling efficiency (*19, 24–26*). This would permit one to select larger slices. It also helps to reduce the RF heating effect that is severe in conductive samples. Third, coil designs with lower RF heating would allow one to shorten the recycle time in the experiment (see Experimental) or to increase the decoupling power. Further work is in progress to investigate this question.

Surfactant diffusion is an ideal tool for providing some answers on the extent and the form of the topological changes of surfactant aggregates upon phase transition. Previously, however, surfactant diffusion coefficients were difficult to measure and there were only a handful of such examples in a few selected liquid crystal phases. Measurements in the vicinity of a phase transition have not yet been presented. This situation is remedied here and, together with the previously published method that uses heteronuclear decoupling with PGSE (*17*), we demonstrated viable experiments for such investigations. More detailed data obtained on phase transitions in lyotropic liquid crystals will be communicated elsewhere.

## EXPERIMENTAL

Cesium perfluorooctanoate was synthesized as described previously (*36*). The liquid crystal sample was produced by mixing CsPFO (50 wt%) with $D_2O$. The isotropic–nematic and nematic–lamellar phase transition temperatures were established from the $^2H$ spectrum to 320 and 314 K, respectively, which agree well with those of the previously established phase diagram (*30*). The nematic phase director orients parallel to the external magnetic field (*37*).

The measurements were performed on a Bruker DMX 200 spectrometer, operating at 188 MHz for $^{19}F$. We used a home-built probe whose exchangeable gradient set-up includes quadrupole gradient coils with gradient directions parallel or perpendicular to the static magnetic field as described previously (*38*). Note that the present gradient direction $x$ is radial for the cylindrical sample space. The probe, double tuned to $^2H$–$^{19}F$ frequencies at 4.7 T field strength, contains a single 6-mm-id and 17-mm-long RF solenoid, made of five turns of flat wire. The lengths of the $^{19}F$ 90° pulse were 2.6 $\mu$s (with 300 W irradiation power). The sample resided in a 5-mm-od and 12-mm-long sealed glass ampule. The gradient coils were driven by a Bruker BAFPA-40 current generator. The current in the present experiments did not exceed 6 A. The gradient strength was calibrated earlier (*17*). The Gaussian-shape selective inversion (70 $\mu$s) RF pulses of 20-kHz bandwidth were truncated at 2% of their peak amplitude. The effect of eddy currents is reduced via including a LED (*31*) extension. A routine phase cycle (first pulse $+x$, $-x$; second and third pulses $2(+x)$, $2(+y)$, $2(-x)$, $2(-y)$; fourth and fifth pulses

$8(+x)$, $8(-x)$; receiver $+x$, $2(-x)$, $2(+x)$, $2(-x)$, $+x$) was applied. Each cycle is repeated twice with and without selective inversion pulse (with phase $+x$) and receiver phase is inverted for subsequent cycles. The pulse phases in the MREV-8 sequence were set to $+x$, $+y$, $-y$, $-x$, $-x$, $+y$, $-y$, $+x$ and were not cycled. The MREV-8 sequence has been sandwiched as $(45°)_{-y}$–(MREV-8)–$(45°)_{+y}$. The 45° pulses align the precessing magnetization perpendicular to the effective field at the beginning of the MREV-8 pulse train and realign it back to the $XY$ plane at the end (*22*, *24*, *25*). This arrangement prevents spin-locking a part of the magnetization parallel to the tilted effective field of the MREV-8 cycle and losing a part of the signal caused by the 45° tilt of the precession plane to the $XY$ plane.

Up to 64 transients (preceded by 16 dummy scans) were accumulated for each individual spectrum of the diffusion experiment. The average temperature was observed and regulated with an accuracy of 0.1 K by the Bruker BVT-3000 unit supplied with the spectrometer. Temperature shift and temperature gradient within the sample caused by the RF irradiation for decoupling were calibrated by observing the splitting and broadening of the temperature-sensitive $^2$H NMR spectra (*30*) of $D_2O$ in the sample. In the diffusion experiments, a recycle delay of 16 s (much longer than required for full spin relaxation) was used to allow for sufficient heat dissipation. Heating effects during the encoding/decoding periods amount to about 0.3 K average temperature spread and about 0.2 K average temperature shift. These temperature shifts were not corrected for in this study.

## ACKNOWLEDGMENTS

This work was supported by the Swedish Natural Science (NFR) and Engineering Science (TFR) Research Councils and the Carl Trygger Foundation. S. V. D. thanks the Wenner-Gren Foundations for a scholarship.

## REFERENCES

1. E. O. Stejskal and J. E. Tanner, Spin diffusion measurements: Spin echoes in the presence of a time-dependent field gradient, *J. Chem. Phys.* **42,** 288–292 (1965).
2. J. E. Tanner, Use of the stimulated echo in NMR diffusion studies, *J. Chem. Phys.* **52,** 2523–2526 (1970).
3. P. Stilbs, Fourier Transform pulsed-gradient spin-echo studies of molecular diffusion, *Prog. Nucl. Magn. Reson. Spectrosc.* **19,** 1–45 (1987).
4. P. T. Callaghan, "Principles of Nuclear Magnetic Resonance Microscopy," Clarendon Press, Oxford (1991).
5. W. S. Price, Pulsed-field gradient nuclear magnetic resonance as a tool for studying translational diffusion: Part I. Basic theory, *Concepts Magn. Reson.* **9,** 299–336 (1997).
6. W. S. Price, Pulsed-field gradient nuclear magnetic resonance as a tool for studying translational diffusion: Part II. Experimental aspects, *Concepts Magn. Reson.* **10,** 197–237 (1998).
7. R. Blinc, J. Pirs, and I. Zupancic, Measurement of self-diffusion in liquid crystals by a multiple-pulse NMR method, *Phys. Rev. Lett.* **30,** 546–549 (1973).
8. M. S. Crawford, B. C. Gerstein, A. L. Kuo, and C. G. Wade, Diffusion in rigid bilayer membranes. Use of combined multiple pulse and multiple pulse gradient techniques in nuclear magnetic resonance, *J. Am. Chem. Soc.* **102,** 3728–3732 (1980).
9. I. Chang, G. Hinze, G. Diezemann, F. Fujara, and H. Sillescu, Self-diffusion coefficient in plastic crystals by multiple-pulse NMR in large static field gradients, *Phys. Rev. Lett.* **76,** 2523–2526 (1996).
10. I. Chang, F. Fujara, B. Geil, G. Hinze, H. Sillescu, and A. Tölle, New perspectives of NMR in ultrahigh static magnetic field gradients, *J. Non-Cryst. Solids* **172–174,** 674–681 (1994).
11. G. J. Krüger, H. Spiesecke, and R. Weiss, A simple spin echo measurement of the anisotropy of the self-diffusion coefficient in a smectic A and B type liquid crystal, *Phys. Lett. A* **51,** 295–296 (1975).
12. S. B. W. Roeder, E. E. Burnell, A. L. Kuo, and C. G. Wade, Determination of the lateral diffusion coefficient of potassium oleate in the lamellar phase, *J. Chem. Phys.* **64,** 1848–1849 (1976).
13. G. Lindblom and H. Wennerström, Amphiphile diffusion in model membrane systems studied by pulse NMR, *Biophys. Chem.* **6,** 167–171 (1977).
14. G. J. Krüger, Diffusion in thermotropic liquid crystals, *Phys. Rep.* **82,** 229–269 (1982).
15. W. Zhang and D. G. Cory, First direct measurement of the spin diffusion rate in a homogeneous solid, *Phys. Rev. Lett.* **80,** 1324–1327 (1998).
16. M. Zhou and L. Frydman, Pulsed-gradient spin-echo measurements of anisotropic diffusion by dipole-decoupled $^{13}$C nuclear magnetic resonance, *Sol. State Nucl. Magn. Reson.* **4,** 301–307 (1995).
17. S. V. Dvinskikh, R. Sitnikov, and I. Furó, $^{13}$C PGSE NMR experiment with heteronuclear dipolar decoupling to measure diffusion in liquid crystals and solids. *J. Magn. Reson.* **142,** 102–110 (2000).
18. M. Mehring, "Principles of High Resolution NMR in Solids," Springer, Berlin (1983).
19. D. P. Burum, M. Linder, and R. R. Ernst, Low-power multi-pulse line narrowing in solid-state NMR, *J. Magn. Reson.* **44,** 173–188 (1981).
20. A. Bielecki, A. C. Kolbert, H. J. M. de Groot, R. G. Griffin, and M. H. Levitt, Frequency-switched Lee–Goldburg sequences in solids, *Adv. Magn. Reson.* **14,** 111–124 (1990).
21. D. G. Cory, A new multiple-pulse cycle for homonuclear dipolar decoupling, *J. Magn. Reson.* **94,** 526–534 (1991).
22. T. M. Barbara and L. Baltusis, Phase-cycled, multiple-window-acquisition, multiple-pulse NMR spectroscopy, *J. Magn. Reson. A* **106,** 182–187 (1994).
23. M. Hohwy and N. C. Nielsen, Elimination of high order terms in multiple pulse nuclear magnetic resonance spectroscopy: Application to homonuclear decoupling in solids, *J. Chem. Phys.* **106,** 7571–7586 (1997).
24. H. Cho, Tilted-axis precession and phase-sensitive detection of nuclear magnetization, *J. Magn. Reson. A* **121,** 8–22 (1996).
25. H. Cho, Off-resonance multiple-pulse dynamics in solid-state NMR spectroscopy: A revised coherent averaging theory analysis, *J. Magn. Reson.* **141,** 164–179 (1999).
26. D. G. Cory and W. S. Veeman, Application of line narrowing to $^1$H NMR imaging of solids, *J. Magn. Reson.* **84,** 392–397 (1989).

*27.* G. C. Chingas, J. B. Miller, and A. N. Garroway, NMR images of solids, *J. Magn. Reson.* **66,** 530–535 (1986).

*28.* D. G. Cory, Solid state NMR imaging, *Annu. Rep. NMR Spectr.* **24,** 87–180 (1992).

*29.* I. Chang, G. Diezemann, G. Hinze, R. Böhmer, and H. Sillescu, Far-off-resonance averaging of dipolar interactions in solids, *J. Magn. Reson.* **124,** 165–171 (1997).

*30.* N. Boden, S. A. Corne, and K. W. Jolley, Lyotropic mesomorphism of the cesium pentadecafluorooctanoate/water system: High-resolution phase diagram, *J. Phys. Chem.* **91,** 4092–4105 (1987).

*31.* S. J. Gibbs and C. S. Johnson, A PFG NMR experiment for accurate diffusion and flow studies in the presence of eddy currents, *J. Magn. Reson.* **93,** 395–402 (1991).

*32.* D. P. Weitekamp, Time-domain multiple-quantum NMR, *Adv. Magn. Reson.* **11,** 111–277 (1983).

*33.* M. Munowitz and A. Pines, Principles and application of multiple-quantum NMR, *Adv. Chem. Phys.* **66,** 1–153 (1985).

*34.* L. Emsley, Selective pulses, *in* "Encyclopedia of Nuclear Magnetic Resonance" (D. M. Grant and R. K. Harris, Eds.), pp. 4228–4236, Wiley, NY (1996).

*35.* R. Raulet, I. Furó, J. Brondeau, B. Diter, and D. Canet, Water-surfactant contact studied by $^{19}F$–$^{1}H$ heteronuclear Overhauser effect spectroscopy, *J. Magn. Reson.* **133,** 324–329 (1998).

*36.* H. Jóhannesson, I. Furó, and B. Halle, Orientational order and micelle size in the nematic phase of the cesium pentadecafluorooctanoate-water system from the anisotropic self-diffusion of water, *Phys. Rev. E* **53,** 4904–4917 (1996).

*37.* N. Boden, G. R. Hedwig, M. C. Holmes, K. W. Jolley, and D. Parker, Anomalous effects in experiments on monodomain nematic and lamellar phases of the caesium pentadecafluoroocatnoate (CsPFO)/water system, *Liq. Cryst.* **11,** 311–324 (1992).

*38.* I. Furó and H. Jóhannesson, Accurate anisotropic water diffusion measurements in liquid crystals, *J. Magn. Reson. A* **119,** 15–21 (1996).